Modelling of magnetic nozzle thrusters with application to ECR and Helicon thrusters

IEPC-2015-359／ISTS-2015-b-359

Presented at Joint Conference of 30th International Symposium on Space Technology and Science, 34th International Electric Propulsion Conference and 6th Nano-satellite Symposium
Hyogo-Kobe, Japan
July 4–10, 2015

Trevor Lafleur*
Ecole Polytechnique, Palaiseau, 91128, France
ONERA - The French Aerospace Lab, Palaiseau, 91120, France

Denis Packan†, Félix Cannat‡, Julien Jarrige§, and Paul-Quentin Elias¶
ONERA - The French Aerospace Lab, Palaiseau, 91120, France

Interest in electrodeless thrusters making use of magnetic nozzles has rapidly increased over the last few years due to inherent advantages of these systems which do not require hollow cathode neutralizers, or accelerating grids. These thrusters are however complex systems, and there is a strong coupling between the plasma production and ion acceleration mechanisms. Here we present a theoretical model that has been developed to rapidly predict the performance and parameter scalings for these thrusters, and we compare it to a range of experimental measurements for a number of different electrodeless thruster systems. In particular, the model is applied to a new electron cyclotron resonance thruster currently being developed at ONERA.

*Postdoctoral research fellow, Laboratoire de Physique des Plasmas, trevor.lafleur@lpp.polytechnique.fr
†Research Scientist, Physics and Instrumentation Department, denis.packan@onera.fr
‡PhD student, Physics and Instrumentation Department, felix.cannat@onera.fr
§Research Scientist, Physics and Instrumentation Department, julien.jarrige@onera.fr
¶Research Scientist, Physics and Instrumentation Department, paul-quentin.elias@onera.fr

Nomenclature

a = Model normalized parameter
A_0 = Cross-sectional area of the plasma source
b = Model normalized parameter
B_e = Magnetic field strength at the source exit
B_s = Average magnetic field strength in the source
E_i = Maximum ion energy
F_0 = Thrust due to plasma pressure on the backwall of the source
F_T = Total thrust
h_R = Edge-to-center plasma density ratio
I_B = Ion beam current
J = Ion current density
K_{iz} = Ionization rate factor
K_{exc} = Excitation rate factor
L = Source length
m = Electron mass
M = Ion mass
M_{det} = Ion Mach number at detachment
$\dot{m}$ = Neutral gas mass flow rate
$\dot{m}^+$ = Ion mass flow rate
n_0 = Maximum plasma density
P_{abs} = Absorbed power
P_T = Total power
q = Elementary charge
r_{ci} = Ion gyroradius
R = Source radius
R_{ant} = Antenna radius
T_e = Electron temperature
T_i = Ion temperature
u_B = Bohm velocity
v_g = Neutral gas velocity
v_i = Ion speed
v_{Ti} = Ion thermal speed
β = Radially-averaged normalized plasma density
γ = Normalized plasma parameter
$\varepsilon_e, \varepsilon_i$ = Electron or ion energy
η_D = Divergence efficiency
η_m = Propellant utilization
η_{rf} = Power transfer efficiency
θ = Angular position
ξ = Normalized plasma parameter
ω_{ci} = Ion cyclotron frequency

I. Introduction

Hall thrusters (HTs) and gridded ion thrusters (GITs) are some of the most successful and widely used electric propulsion systems to date, and have been continuously developed for the last 50 years.[1] Both thrusters operate in a nominally dc mode, and accelerate ions to high energy by making use of biased electrodes. Hollow cathode electron emitters are used to both produce the plasma in HTs and some GITs, as well as to emit sufficient electrons to ensure current equality and charge compensation of the ion beam in the downstream region. These hollow cathodes however require separate power supplies and gas feeds, and represent a life-limiting component of these systems.[1] In addition, the ion acceleration grids in GITs suffer erosion due to ion bombardment because of charge exchange collisions, while the walls of Hall thrusters can suffer erosion if not properly shielded.

A number of different thruster concepts[2–11] have been proposed that function in a different manner to HTs and GITs, and which do not suffer from the above problems. These systems make use of a plasma which is produced in an upstream source, and then expanded through a magnetic nozzle in the downstream region. As the plasma expands, ambipolar electric fields are formed which ensure equal currents of positive ions and electrons leave the thruster, and these fields accelerate ions to generate thrust. There are no accelerating electrodes needed, and sufficient high energy electrons are able to escape the source to ensure a quasi-neutral plasma exhaust. As a result, no hollow cathode neutralizer is needed, and the system can be made very compact. In addition, the presence of the magnetic field can help to shield the walls of the plasma source to reduce erosion.

Two main types of expanding-plasma thrusters have been developed: (a) electron cyclotron resonance (ECR) thrusters,[2–5,12,13] and (b) helicon thrusters.[7–9] ECR thrusters make use of microwaves and produce a plasma due to electron cyclotron resonance in an applied magnetic field. This field is usually produced with a set of solenoids, and so naturally diverges in the downstream region creating a magnetic nozzle. The magnetic field in these systems is relatively high (about 900 G to have a resonance at 2.45 GHz), and so the thruster radial side walls can be shielded if the magnetic field is properly designed. Helicon thrusters operate in a similar manner, except that the plasma is produced by helicon waves, which are a type of electromagnetic wave launched from an rf antenna (usually operated at 13.56 MHz) surrounding a dielectric plasma source.

The physics in these expanding-plasma thrusters is however complex,[14–17] and because of the lack of a separate acceleration region, the plasma production and acceleration are strongly coupled, as is the power transfer from the antenna to the plasma. This creates challenges for understanding and predicting the performance, and for knowing the relevant scaling laws to help design optimized systems. A theoretical model[16] has been developed that allows the behaviour of many aspects of these systems to be understood, and which provides a simple method for providing an estimate of thruster performance without needing to resort to numerical simulations. Here we briefly review this model, and demonstrate its application to a number of ECR and helicon thrusters.

II. Model description

A. Plasma source

This model has been presented before in Refs.,[12,16] and here we provide just a brief overview. We consider a plasma source region, as well as a downstream magnetic nozzle region (see Fig. 1). In the source region we use a quasi-2D model where we assume a radial plasma density profile, but whose shape changes depending on the strength of the applied magnetic field (see below). The radial neutral gas density profile is assumed uniform, but both the axial plasma density and axial neutral gas density variation is determined self-consistently. Thus the model accounts for neutral gas depletion in the presence of strong ionization. Electrons are assumed isothermal, while ions are cold and collisionless, and reach the Bohm velocity at the source exit. By then combining the relevant continuity and momentum conservation equations,[16] the electron temperature is found from the normalized equation

$$-2-\xi\ln\left(\frac{1-\xi}{1+\xi}\right)+2\sqrt{1-\xi^2}\left[\arctan\left(\frac{1-\xi}{\sqrt{1-\xi^2}}\right)-\arctan\left(\frac{-1-\xi}{\sqrt{1-\xi^2}}\right)\right]=\gamma \tag{1}$$

where

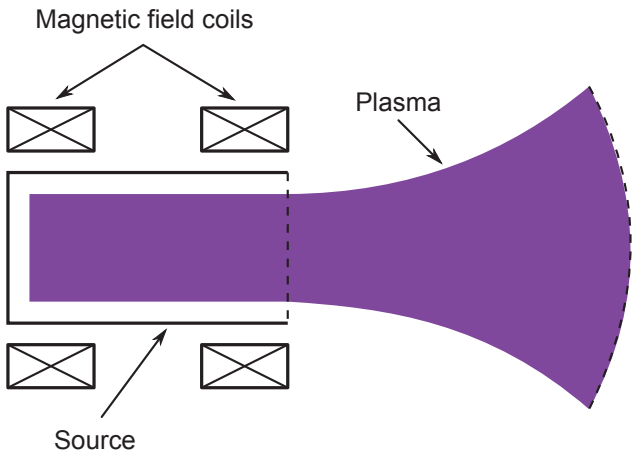

Figure 1. Schematic of the thruster model showing the plasma source region and the downstream magnetic nozzle.

$$\gamma = a\frac{K_{iz}}{u_B} - b \tag{2}$$

$$\xi = \frac{\eta_m}{1 - \frac{u_B}{K_{iz}}\frac{b}{a}} \tag{3}$$

$$a = \frac{\dot{m}L}{Mv_gA_0} \tag{4}$$

$$b = \frac{2h_RL}{\beta R} \tag{5}$$

$$\eta_m = \frac{M\beta n_0 u_B A_0}{2\dot{m}} \tag{6}$$

Here $K_{iz} = K_{iz}(T_e)$ is the ionization rate factor, $u_B = \sqrt{qT_e/M}$ is the Bohm velocity with q the elementary charge, T_e the electron temperature (in units of [eV]), and M the ion mass, η_m is the propellant utilization, $\dot{m}$ is the total neutral gas mass flow rate into the thruster, L and R are the length and radius of the plasma source, v_g is the neutral gas velocity (assumed equal to the speed of sound), A_0 is the cross-sectional area of the source exit, and n_0 is the maximum plasma density in the source. The parameter, h_R, represents the level of plasma confinement due to the applied magnetic field, and is found using a semi-empirical cross-field diffusion model to account for anomalous transport

$$h_R \approx \frac{0.4}{\sqrt{1 + 0.68\left(R/r_{ci}\right)^2}} \tag{7}$$

where $r_{ci} = v_{Ti}/\omega_{ci}$ is the ion cyclotron radius with $v_{Ti} = \sqrt{qT_i/M}$ the ion thermal speed, T_i the ion temperature, $\omega_{ci} = qB_s/m_i$ the ion cyclotron frequency, and B_s the average magnetic field inside the thruster. The parameter, β, in Eqn. 5 represents a measure of the radially-averaged plasma density, and is given by

$$\beta = \frac{1}{7\left(1 - h_R^{1/6}\right)}\left(\left[\left(1 - h_R^{1/6}\right) - 1\right]^7 + 1\right) \tag{8}$$

Because neutral depletion occurs at high plasma densities, Eqn. 1 for the electron temperature needs to be solved simultaneously with an equation for the plasma power losses in the source, which can be expressed as

$$\begin{aligned} P_{abs} = \frac{1}{2}q\beta n_0 u_B A_0\left(\varepsilon_c + \varepsilon_{ic} + \varepsilon_{ec}\right) \quad &+ \quad \frac{1}{2}q\beta n_0 u_B A_0\left(\varepsilon_c + \varepsilon_{io} + \varepsilon_{eo}\right) \\ &+ \quad \frac{\pi q R h_R n_0 L}{\gamma\xi}\ln\left(\frac{1+\xi}{1-\xi}\right) u_B\left(\varepsilon_c + \varepsilon_{ir} + \varepsilon_{er}\right) \end{aligned} \tag{9}$$

Here P_{abs} is the power absorbed by the plasma, $\varepsilon_c = \varepsilon_{ion} + \frac{K_{exc}}{K_{iz}}\varepsilon_{exc}$ is the collisional energy loss (ε_{ion} is the ionization energy, while ε_{exc} is the excitation energy), K_{exc} is the excitation rate factor, $\varepsilon_{ic} = \varepsilon_{io} = \varepsilon_{ir} = \varepsilon_i = \frac{T_e}{2}$ is the ion kinetic energy at the sheath edges, $\varepsilon_{ec} = \varepsilon_{er} = \varepsilon_e = 2T_e + \frac{T_e}{2}\ln\left(\frac{M}{2\pi m}\right)$ is the electron energy loss on the walls, and $\varepsilon_{eo} = \frac{1}{2}M_{det}^2 T_e + 2T_e$ is the electron energy loss at the source exit, with M_{det} the ion Mach number at detachment (see Section II B).

The above model applies for a cylindrical plasma source. For a coaxial geometry, such as that used in the ECR thruster in Section III C, the equations are slightly modified[12] to account for plasma losses on the inner antenna surface, which has a radius of R_{ant}. However, as long as $R_{ant} << R$, the difference compared with the cylindrical model is only a few percent.

B. Magnetic nozzle and total thrust

By assuming a collisionless plasma in the downstream magnetic nozzle region, the continuity and momentum conservation equations can again be combined to obtain an expression for the total thrust of the system,[16] which includes contributions from both the magnetic nozzle itself, as well as the force on the backwall of the plasma source

$$F_T = \left(\frac{M_{det}^2 + 1}{2M_{det}}\right) F_0 \tag{10}$$

where

$$F_0 = q\beta n_0 T_e A_0 \tag{11}$$

At some point downstream the plasma is assumed to stop expanding in the magnetic nozzle, and detach from the field lines. We assume this occurs when the ions demagnetize,[18] and the ion Mach number at this point is found numerically by solving

$$\frac{1}{2}\left(M_{det}^2 - 1\right) - \ln M_{det} = \ln\left(\frac{qB_e^2 R^2}{MT_i}\right) \tag{12}$$

where B_e is the magnetic field strength at the source exit.

III. Comparison with experiment

With the motivation and model description outlined above, we now apply the model to 3 different electrodeless thrusters, and compare the results to available experimental data.

A. Unmagnetized rf thruster

Here we model the two rf thrusters described in Ref.[10] These systems do not have an applied magnetic field, and so when the plasma exits the source, it simply expands into vacuum. Both thrusters have a source radius of 3.2 cm, lengths of 17.5 cm and 9.5 cm, and argon mass flow rates of 0.9 mg/s and 1.65 mg/s respectively. In Ref.[10] the thrust for these systems was directly measured using a pendulum thrust balance, and the results, together with the model predictions, are shown in Fig. 2. As seen, the model is in good agreement with the data for both thrusters, and displays similar thrust scaling with applied rf power. Note that the neutral gas thrust was not measured in these experiments (because the gas inlet is not connected to the thrust balance), and so has not been included in the model.

B. Helicon thruster

A number of helicon thrusters being developed by different groups has been reported in the literature. Here we choose to focus on the thrusters in Ref.[19] Operation of rf thrusters in a vacuum environment is

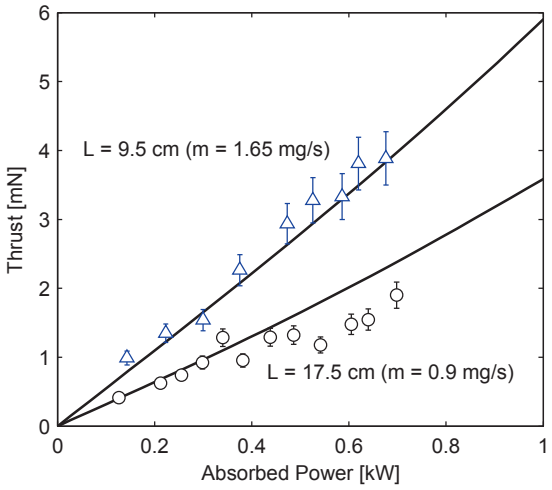

Figure 2. Thrust as a function of absorbed power for two unmagnetized rf thrusters. The solid lines show the model results, while the data points are taken from Ref.[10] The error bars are estimated based on the data in Ref.[10]

challenging, because any residual gas in the vacuum chamber due to the finite pumping speed can result in plasma breakdown around the rf antenna, and the formation of a secondary parasitic plasma which acts as both a sink for power, and distorts the downstream plasma density profiles (and hence magnetic nozzle thrust). The rf antennas in the thrusters of Ref.[19] have been specially shielded to minimise these effects. The thruster has a source radius of 3.25 cm, a length of 12 cm, and an argon mass flow rate of 0.72 mg/s. Two magnetic field strengths were tested, with average values of 63 G and 172 G, and exit values of 112 G and 269 G respectively. The directly measured thrust and model results are shown in Fig. 3. In the experiment the total power from the rf generator was measured, P_T, which is related to the absorbed power by, $P_{abs} = \eta_{rf} P_T$, where η_{rf} is the coupling efficiency between the antenna and the plasma. For the low and high magnetic field strength cases, the coupling efficiency was 75% and 90% respectively. As seen in Fig. 3, the model results are in very good agreement with the measured thrust, and almost exactly reproduce the variation with applied power.

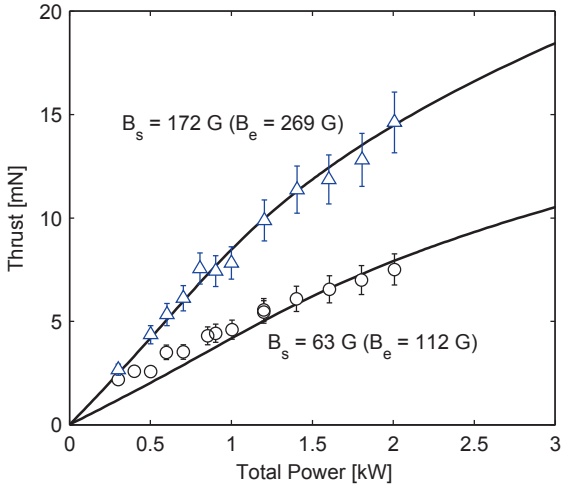

Figure 3. Thrust as a function of total applied power for two helicon thrusters. The solid lines show the model results, while the data points are taken from Ref.[19] The error bars are estimated based on the data in Refs.[10, 19]

C. ECR thruster

ONERA is currently developing a new ECR microwave thruster that has been previously described.[4,5,12] The thruster consists of a coaxial geometry with a central microwave antenna operating at 2.45 GHz. Two versions of the thruster have been tested: a version with a radius of 6.5 mm, a length of 15 mm and a magnetic field produced by a set of permanent magnets, and a larger version with a radius of 13.5 mm, lengths between $15-18$ mm, and a magnetic field produced with a solenoid. The antenna radius is 0.9 mm. The thruster is placed within a large 1 m diameter, 4 m long, vacuum chamber with cryogenic pumps. The system is then characterised with a number of electrostatic probes to determine the plasma properties, and estimate the thrust for a range of operating conditions.

1. *Electron temperature*

The electron temperature is measured outside the thruster with a Langmuir probe, and is determined from the electron energy probability function (EEPF), which is obtained from the second derivative of the measured probe current with bias voltage.[20] Figure 4 shows the measured temperature, as well as the model predictions, for different thruster configurations operated with both argon and xenon, while Fig. 5 shows the results for the larger thruster at different magnetic field strengths. Good agreement is found, particularly for argon, and the same scaling with mass flow rate is observed. The model results are slightly shifted for the xenon results, which is most likely due to increased neutral gas heating which is not accounted for in the model.

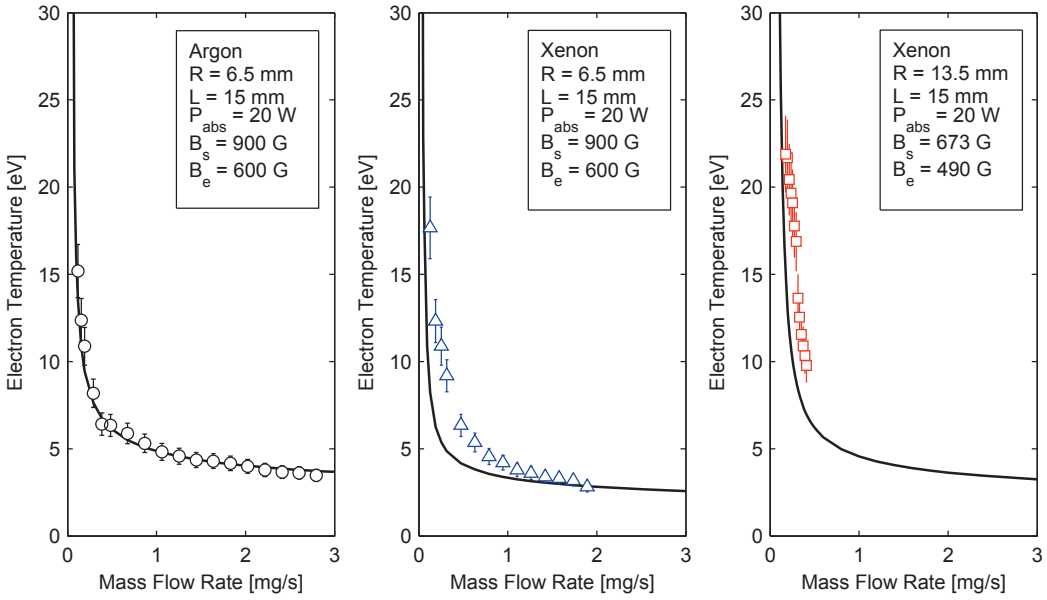

Figure 4. Electron temperature as a function of neutral gas mass flow rate for different operating conditions. The solid lines show the model results, while the markers show experimental measurements taken from Ref.[12]

2. *Ion beam current*

The ion beam current, I_B, is obtained by taking angular measurements of the ion current density, $J(\theta)$ with a single-grid Faraday probe placed on a rotation stage.[12] The total ion current is found by integrating the angular profile

$$I_B = \int_0^{\pi} J(\theta) \sin\theta d\theta \tag{13}$$

Figure 6 shows the measured and predicted ion beam current for a number of different operating conditions. The agreement is quite reasonable, although the model tends to over predict the beam current; most likely because of the under predicted electron temperature, as highlighted in Section III C 1.

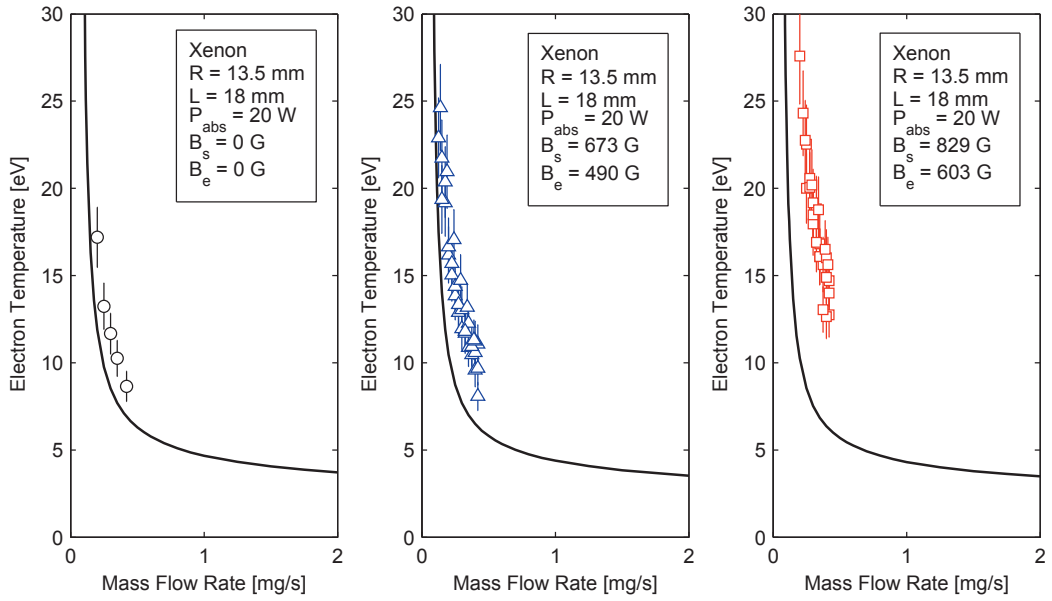

Figure 5. Electron temperature as a function of neutral gas mass flow rate for different magnetic field strengths. The solid lines show the model results, while the markers show experimental measurements.

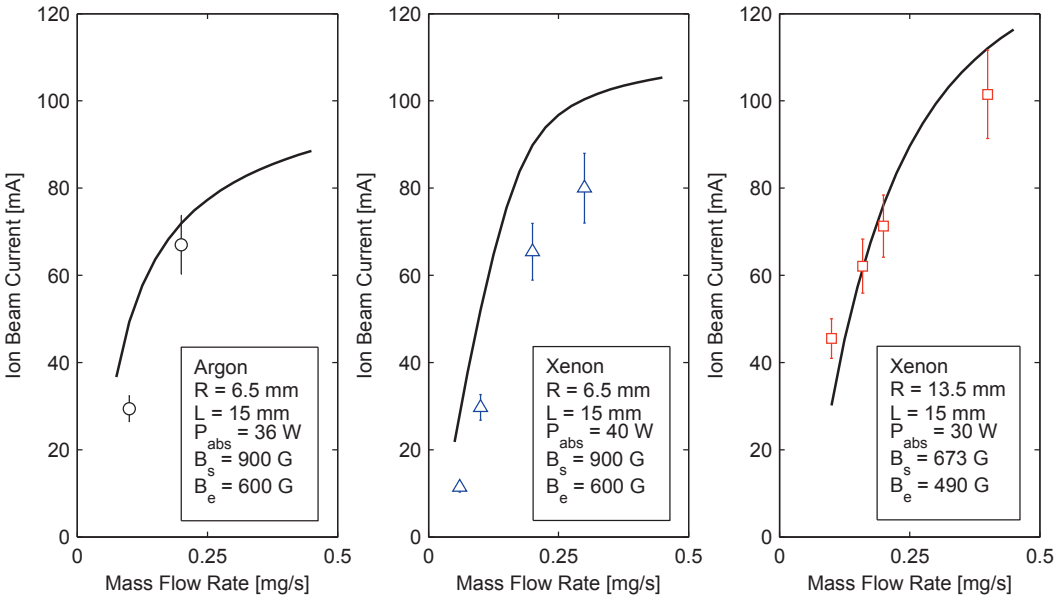

Figure 6. Ion beam current as a function of neutral gas mass flow rate for different operating conditions. The solid lines show the model results, while the markers show experimental measurements taken from Ref.[12]

3. Thrust

The thrust in the experiment is found from

$$F_T = \eta_D \dot{m}^+ v_i \tag{14}$$

where $\dot{m}^+ = MI_B/q$ is the ion mass flow rate, $v_i = \sqrt{2qE_i/M}$ is the final ion speed with E_i the final ion energy, and η_D a factor to account for ion beam divergence, and which is found from

$$\eta_D = \frac{\int_0^\pi J(\theta) \sin\theta \cos\theta d\theta}{\int_0^\pi J(\theta) \sin\theta d\theta} \tag{15}$$

The ion energy is measured using a Hiden mass spectrometer, and checked with a retarding field energy analyzer. The experimental and theoretical thrusts are shown in Fig. 7 for different operating conditions. The results are in reasonable agreement, with the model thrusts slightly lower than those measured experimentally. Since the thrust depends on the electron temperature from Eqn. 10, the under predicted thrust is again due to the under predicted electron temperature discussed in Section III C 1.

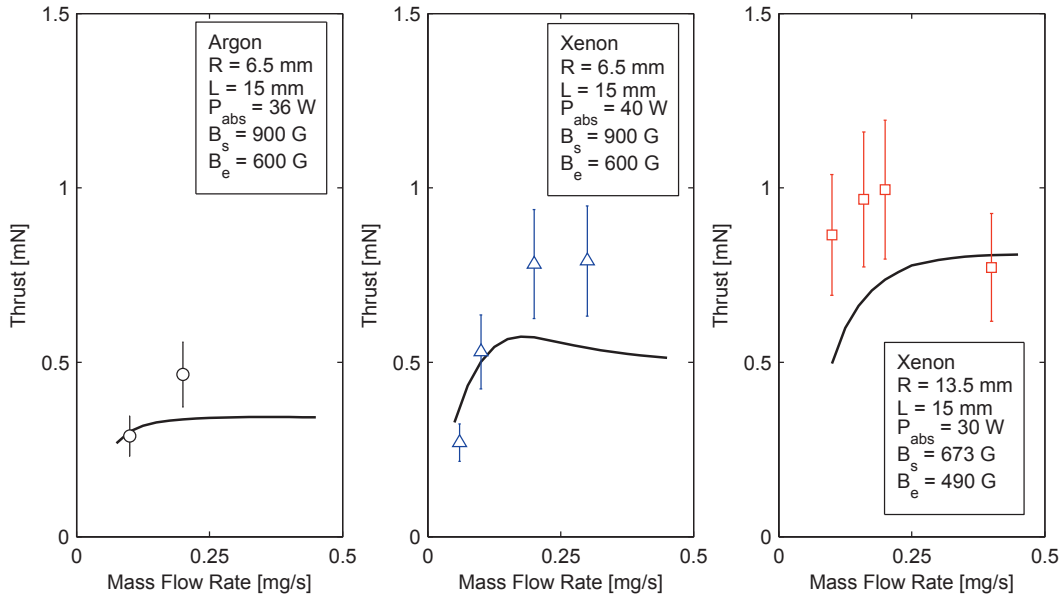

Figure 7. Thrust as a function of neutral gas mass flow rate for different operating conditions. The solid lines show the model results, while the markers show experimental measurements taken from Ref.[12]

IV. Performance limits

The model for the magnetic nozzle in Section II B is very simple and assumes isothermal electrons. This assumption results in continuous ion acceleration, and an infinite ion energy. We have avoided this problem by assuming that the plasma detaches when the ions demagnetize, which establishes a finite maximum ion energy.

In reality, some form of electron cooling occurs in the downstream,[17] and the maximum ion energy is determined by the requirement that the total current of electrons and ions leaving the thruster be equal. For a Maxwellian electron distribution, this requirement is almost identical to that for a floating sheath,[21] and determines the maximum ion energy as

$$E_i = \frac{T_e}{2}\left[1 + \ln\left(\frac{M}{2\pi m}\right)\right] \tag{16}$$

For xenon this gives, $E_i/T_e \approx 6$. If the electron distribution shows a high-energy depletion, as has been measured in these low pressure discharges,[12] then $4 < E_i/T_e < 6$. Experimental measurements of the ion energy and electron temperature have indeed found values in this range. From Eqn. 1, the equation for the electron temperature depends only on the value, K_{iz}/u_B. This ratio is shown for xenon as a function of electron temperature in Fig. 8, where a maximum value occurs at $T_e \approx 65$ eV. Thus from Eqn. 16, the maximum achievable ion energy is about 400 eV. Values close to this have previously been experimentally measured.[4,5] Thus by using the model in Section II A, together with Eqn. 16 and Eqn. 14, a second method exists to estimate the thrust. Two-dimensional numerical simulations,[22] and experimental measurements[12] show that the divergence efficiency, η_D, is typically in the range 70-85%.

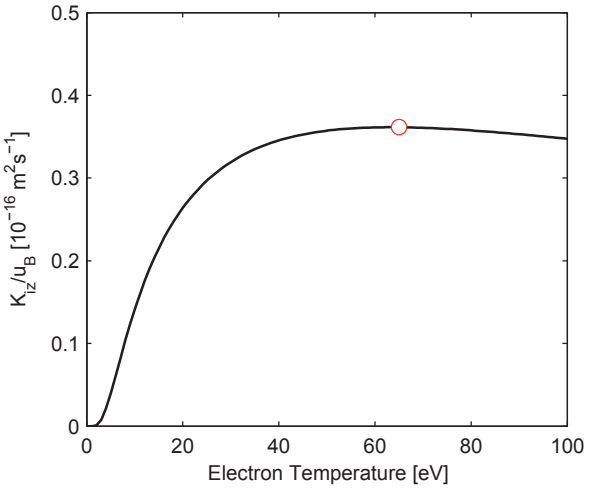

Figure 8. Ratio of K_{iz}/u_B as a function of electron temperature. The red marker denotes the location where K_{iz}/u_B is a maximum.

V. Conclusions

In summary, we have developed an analytical model which has been applied to different electrodeless thrusters, and tested under a large range of different conditions. The model is in quite reasonable agreement with available experimental measurements, and reproduces most of the observed trends. Further improvements to the model could be made by accounting for neutral gas heating inside the plasma source, making use of a more sophisticated model of the magnetic nozzle, and by modelling the antenna-plasma coupling. The model nevertheless serves as a useful tool for making fast, first estimates of thruster performance.

Acknowledgments

This work received financial state aid managed by the Agence Nationale de la Recherche as part of the program “blanc” under the reference ANR-2011-BS09-40 (EPIC), and the program “Investissements d’avenir” under the reference ANR-11- IDEX-0004-02 (Plas@Par).

References

[1]D.M. Goebel and I. Katz, ”Fundamentals of Electric Propulsion: Ion and Hall Thrusters”, Wiley, New Jersey, 2008.

[2]R.G. Jahn, ”Physics of electric propulsion”, McGraw-Hill, New York, 1968.

[3]J.C. Sercel, ”An experimental and theoretical study of the ECR plasma engine”, PhD thesis, Pasadena California Institute of Technology, 1993.

[4]J. Jarrige, P.Q. Elias, F. Cannat, and D. Packan, ”Characterization of a coaxial ECR plasma thruster”, AIAA 2013-2628, *Proceedings of the 44^{t}h AIAA Plasmadynamics and lasers conference*, San Diego, USA, 24-27 June 2013.

[5]J. Jarrige, P.Q. Elias, F. Cannat, and D. Packan, ”Performance comparison of an ECR plasma thruster using argon and xenon as propellant gas”, *Proceedings of the 33th International Electric Propulsion Conference*, AIAA 2013-420, Washington

D.C., USA, 6-10 October 2013.

[6]T. Takahashi, Y. Takao, K. Eriguchi, and O. Kouichi, "Numerical and experimental study of microwave-excited microplasma and micronozzle flow for a microplasma thruster", *Phys. Plasmas*, **16**, 083505, 2009.

[7]K. Takahashi *et al*, "Direct thrust measurements of a permanent magnet helicon double layer thruster", *Appl. Phys. Lett.*, **98**, 141503, 2011.

[8]K. Takahashi, T. Lafleur, C. Charles, and R.W. Boswell, "Electron dimagnetic effect on axial force in an expanding plasma: experiments and theory", *Phys. Rev. Lett.*, **107**, 235001, 2011.

[9]O. Batishchev, "Minihelicon plasma thruster", *IEEE Trans. Plasma Sci.*, **37**, 1563, 2009.

[10]T. Lafleur, K. Takahashi, C. Charles, and R. Boswell, "Direct thrust measurements and modelling of a radio-frequency expanding plasma thruster", *Phys. Plasmas*, **18**, 080701, 2011.

[11]D. Pavarin *et al*, "Design of a 50 W helicon plasma thruster", IEPC-2009-205, *Proceedings of the 31st International Electric Propulsion Conference*, University of Michigan, USA, 20-24 September 2009.

[12]F. Cannat, T. Lafleur, J. Jarrige, P. Chabert, P.Q. Elias, and D. Packan, "Optimization of a coaxial electron cyclotron resonance plasma thruster with an analytical model", *Phys. Plasmas*, **22**, 053503, 2015.

[13]F. Cannat, T. Lafleur, J. Jarrige, P. Chabert, P.Q. Elias, and D. Packan, "Experimental geometry investigation of a coaxial ECR plasma thruster", IEPC-2015-90492, *34st International Electric Propulsion Conference*, Kobe, Japan, 4-10 July 2015.

[14]A. Fruchtman, "Neutral depletion in a collisionless plasma", *IEEE Trans. Plasma Sci.*, *36*, 403, 2008.

[15]4. E. Ahedo and J. Navarro-Cavallé, "Helicon thruster plasma modeling: Two-dimensional fluid-dynamics and propulsive performances", *Phys. Plasmas* **20**, 043512, 2013.

[16]T. Lafleur, "Helicon plasma thruster discharge model", *Phys. Plasmas*, **21**, 043507, 2014.

[17]M. Martinez-Sanchez, J. Navarro-Cavallé, and E. Ahedo, "Electron cooling and finite potential drop in a magnetized plasma expansion", *Phys. Plasmas*, **22**, 053501, 2015.

[18]M. Merino and E. Ahedo, "Plasma detachment in a propulsive magnetic nozzle via ion demagnetization", *Plasma Sources Sci. Technol.*, **23**, 032001, 2014.

[19]K. Takahashi, C. Charles, R. Boswell, and A. Ando, "Performance improvement of a permanent magnet helicon plasma thruster", *J. Phys. D: Appl. Phys.*, **46**, 325001, 2013.

[20]V.A. Godyak, R.B. Piejak, and B.M. Alexandrovich, "Measurement of electron energy distribution in low-pressure rf discharges", *Plasma Sources Sci. Technol.*, **1**, 36, 1992.

[21]M.A. Lieberman and A.J. Lichtenberg, "Principles of plasma discharges and materials processing", John Wiley & Sons, New Jersey, 2005.

[22]M. Merino and E. Ahedo, "Influence of electron and ion thermodynamics on the magnetic nozzle plasma expansion", *IEEE Trans. Plasma Sci.*, **43**, 244, 2014.